Effect of spherical blockage configurations on film cooling

Wang, Jin; Ke, Tian; Zhang, Kai; Baleta, Jakov; Sundén, Bengt

EFFECT OF SPHERICAL BLOCKAGE CONFIGURATIONS ON FILM COOLING

by

Jin WANG[a], *Ke TIAN*[a], *Kai ZHANG*[a, b], *Jakov BALETA*[c], *and Bengt SUNDÉN*[d*]

[a] School of Energy and Environmental Engineering, Hebei University of Technology,
Tianjin, China
[b] School of Energy Power and Mechanical Engineering, North China Electric Power University,
Beijing, China
[c] Department of Energy, Power Engineering and Environment, Faculty of Mechanical Engineering
and Naval Architecture, University of Zagreb, Zagreb, Croatia
[d] Department of Energy Sciences, Division of Heat Transfer, Lund University,
Lund, Sweden

With increasing inlet temperature of gas turbines, turbine blades need to be effectively protected by using cooling technologies. However, the deposition from the fuel impurities and dust particles in the air is often found inside film holes, which results in partial hole blockage. In this paper, the deposition geometry is simplified as a rectangular channel, and the effect of three blockage ratios is investigated by using the computational fluid dynamics. In addition, water droplets are also released from the coolant inlet to provide a comparison of the results with and without mist injection. It is found that the lateral film cooling effectiveness is reduced with increasing blockage ratio. For all the cases with the blowing ratio 0.6, 1% mist injection provides an improvement of the cooling performance by approximately 10%.

Key words: *film cooling, blockage, mist injection, sphere, gas turbine*

Introduction

As an important industrial equipment, gas turbines are used to provide thermal thrust and produce electrical energy. Hot components of gas turbines usually operate at high temperature conditions. Based on the MacCormack's technique, Kumar *et al.* [1] presented the effect of arrangement of ribs and parabolic fins in an internal cooling channel, and they found that the channel with parabolic fins provided a lower temperature distribution on the blade surface. To improve the operation efficiency and reduce the emissions, many cooling technologies are adopted to protect the vanes/blades from excessive thermal loads due to increasing turbine inlet temperature. Liu and Zheng [2] conducted fluid-solid coupling simulations to investigate performance of effusion cooling in the real combustion chamber condition. Xie *et al.* [3] investigated film cooling performance of a 3D model of the trailing edge cooling channel, and results showed that increasing the blowing ratio have significant contribution to protection of the trailing edge.

Koc *et al.* [4] conducted a numerical investigation of the film cooling effectiveness on various curved surfaces. They found that the film cooling effectiveness depends on the

---

* Corresponding author; e-mail: bengt.sunden@energy.lth.se

optimum selection of the blowing ratio and maximum curvature height. Asghar and Hyder [5] carried out a computational analysis of the average film cooling effectiveness using a row of semi-circular holes, and it was found that the centerline and lateral effectiveness values from two staggered rows of semi-circular holes were much higher than those from a single row of full circular holes. By considering effects of five inclination angles and four blowing ratios, Bayraktar and Yilmaz [6] found that a maximum value of the cooling efficiency was obtained at an inclination angle of 30° and a blowing ratio of 2.0. Shine *et al.* [7] showed that a higher tangential orientation of the coolant jet with the mainstream resulted in lower effectiveness in the test section. Du and Li [8] investigated effects of slot injection configuration and endwall film cooling using the shear stress transport (SST) k-ω turbulence model. The results indicated that the coolant coverage area extended when the slot width decreased.

In the actual working conditions, operating efficiency of equipment is significantly affected by particle deposition. Liu and Hao [9] numerically and experimentally investigated deposition characteristics in the entrained flow coal gasifier, and they found that the deposition process should be divided into two parts, collision and backflow. Chung *et al.* [10] indicated that a perforated blockage configuration with an inclined hole array obviously improved the cooling performance by using the naphthalene sublimation method. However, it is well known that the film cooling characteristics are affected by the surface deposition and the hole blockage for the turbine blades. Davidson *et al.* [11] studied the deposition on a turbine vane with thermal barrier coatings. It was found that the film cooling significantly accelerated the deposition accumulation. Kistenmacher *et al.* [12] experimentally found that a two-trench design obviously reduced the deposition compared to a round-hole configuration. Li and Wang [13] investigated the adiabatic cooling effectiveness with mist injection in a rectangular channel, and they found that better cooling performance can be obtained by decreasing the droplet diameter and increasing the mist concentration. Wang *et al.* [14] analyzed the effect of different deposition locations on film cooling with mist injection, and they found that the deposition located far away the film hole will improve the film cooling effectiveness. Wang *et al.* [15] investigated the effect of deposition configurations with and without mist injection on film cooling. The results showed that the mist injection increased the film cooling effectiveness downstream the wall. Wang *et al.* [16] also showed that the cooling performance was improved by decreasing the deposition height.

Recently, some researchers focused attention on the partial hole blockage, and how the blockage configuration reduces the film cooling effectiveness. Pan *et al.* [17] numerically investigated the effect of partial blockage inside cylindrical film holes by using a three-dimensional model. The primary vortices were weakened by the partial blockage near the coolant hole. Based on the experimental results from an infrared camera, Yang and Zhang [18] found that the coolant jet flow was deflected by the ridge-shaped tab upstream the hole center. The high cooling effectiveness was achieved by decreasing the blowing ratio for cylindrical film holes. Huang *et al.* [19] investigated effects of the blockage configurations on the adiabatic film cooling effectiveness, and the results showed that partial blockage positioned at the leading edge enhanced the film cooling effectiveness.

Many other researchers conducted experiments or numerical simulations for simple configurations without mist injection. The effect of the hole blockage is numerically investigated by using a spherical configuration inside the cylindrical film hole in this paper. This study aims to investigate the film cooling effectiveness downstream the partially blocked hole. Furthermore, a comparison of results with and without mist injection is conducted at various blowing ratios.

Numerical model

Figure 1 shows the details of the geometry for numerical simulations in this paper. The computational domain has dimensions of $33d \times 10d \times 2d$, and a film hole with an inclination angle of $35°$ is located at $x = 8d$. The diameter of the film hole (d) is 6 mm, and a spherical blockage configuration with a diameter of $0.5d$ is arranged on the side wall of the hole passage. There is a distance of $0.5d$ between the center of the spherical configuration and the outlet of the film hole. The blockage ratio (BR) is calculated by the following equation in [17]:

$$\text{BR} = \frac{4A_{\text{b,section}}\sin\alpha}{\pi d^2} \tag{1}$$

where $A_{\text{b,section}}$ is the cross-sectional area of the spherical blockage parallel to the x-z plane (through the center of the spherical blockage). Various blockage ratios are obtained by changing the distance (e) between the center of the spherical configuration and the passage sidewall. More details can be found in tab. 1.
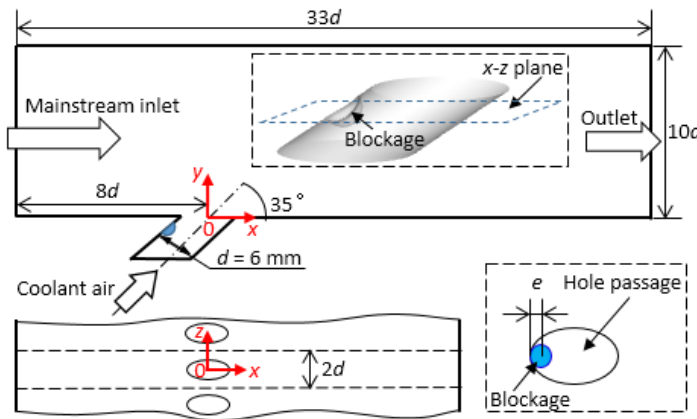

Figure 1. Sketch of the computational domain

Table 1. Dimensions of spherical blockages

Item	Distance e [mm]	BR
Case-S0	–	0%
Case-S1	−0.75	4.5%
Case-S2	0	17%
Case-S3	0.75	25%

Table 2. Boundary conditions

Zone	Type	Value
Mainstream	Velocity-inlet	25 m/s, 338 K
Coolant flow	Velocity-inlet	Air: $M = 0.3, 0.6, 0.9, 1.2$, 300 K Droplets: $2\cdot10^{-5}$ kg/s, 300 K
Outlet	Pressure-outlet	101,325 Pa
Side walls	Symmetry	–
Other walls	No-slip	–

Boundary conditions

Table 2 shows various boundary conditions both for the mainstream and the coolant flow. Uniform temperature distributions are assumed at the inlets with values of 338 K and 300 K for the mainstream and the coolant flow, respectively. Considering the density of the air as a piecewise-linear function of temperature, different velocities of 6.7 m/s, 13.3 m/s, 20 m/s, and 26.6 m/s are set as the inlet velocity of the coolant air. These correspond to the blowing ratios (M) of 0.3, 0.6, 0.9 and 1.2, respectively. The water droplets have a uniform diameter of 10 μm as shown in [13]. The symmetry boundary and no-slip condition are specified to the side walls and other walls, respectively.

Governing equations

The Realizable k-ε turbulence model is adopted to solve the steady-state Navier-

Stokes equations. The discrete phase model (DPM) is used to investigate the interaction between the continuous phase and discrete phase. The governing equations of mass, momentum, energy, the turbulent kinetic energy and the turbulent dissipation rate are presented as follows:

$$\frac{\partial}{\partial x_i}(\rho u_i) = S_m \tag{2}$$

$$\frac{\partial}{\partial x_i}(\rho u_i u_j) = \rho \bar{g}_j - \frac{\partial P}{\partial x_j} + \frac{\partial}{\partial x_i}(\tau_{ij} - \rho \overline{u_i' u_j'}) + F_j \tag{3}$$

$$\frac{\partial}{\partial x_i}(\rho c_p u_i T) = \frac{\partial}{\partial x_i}\left(\lambda \frac{\partial T}{\partial x_i} - \rho c_p \overline{u_i' T'}\right) + |\mu \Phi + S_h| \tag{4}$$

$$\frac{\partial}{\partial x_i}(\rho u_i k) = \frac{\partial}{\partial x_i}\left[\left(\mu + \frac{\mu_t}{\sigma_k}\right)\frac{\partial k}{\partial x_i}\right] + G_k + G_b - \rho \varepsilon \tag{5}$$

$$\frac{\partial}{\partial x_i}(\rho u_i \varepsilon) = \frac{\partial}{\partial x_i}\left[\left(\mu + \frac{\mu_t}{\sigma_\varepsilon}\right)\frac{\partial \varepsilon}{\partial x_i}\right] + \rho C_1 S \varepsilon - \rho C_2 \frac{\varepsilon^2}{k + \sqrt{\nu \varepsilon}} + C_1 \frac{\varepsilon}{k} C_{3\varepsilon} G_b \tag{6}$$

where the gravity is considered in the mist cases. G_k and G_b represent the generation of turbulence kinetic energy due to the mean velocity gradients and buoyancy, respectively. $\mu \phi$ is the dissipation heat, and λ is thermal conductivity. The source terms S_m, F_j, and S_h are used to include the contributions from the dispersed phase. S is the modulus of the mean rate-of-strain tensor. Reynolds stresses, turbulent heat fluxes, symmetric stress tensor and turbulent (or eddy) viscosity are represented by the terms of $\rho \overline{u_i' u_j'}$, $\rho c_p \overline{u_i' T'}$, τ_{ij} and μ_t in the equations above, respectively, as follows:

$$-\rho \overline{u_i' u_j'} = \mu_t \left(\frac{\partial u_i}{\partial x_j} + \frac{\partial u_j}{\partial x_i}\right) - \frac{2}{3}\rho k \delta_{ij} \tag{7}$$

$$\rho c_p \overline{u_i' T'} = -\lambda_t \frac{\partial T}{\partial x_i} = -c_p \frac{\mu_t}{Pr_t} \frac{\partial T}{\partial x_i} \tag{8}$$

$$\tau_{ij} = \mu \left(\frac{\partial u_j}{\partial x_i} + \frac{\partial u_i}{\partial x_j} - \frac{2}{3}\delta_{ij}\frac{\partial u_k}{\partial x_k}\right) \tag{9}$$

$$\mu_t = \rho C_\mu \frac{k^2}{\varepsilon} \tag{10}$$

The model constants have the following default values as given in [20, 21]:

$$[C_{1\varepsilon}, C_{2\varepsilon}, C_\mu, \sigma_k, \sigma_\varepsilon] = [1.44, 1.92, 0.09, 1.0, 1.3] \tag{11}$$

For the mist cases, the evaporation of the water droplets releases water vapor into the mainstream, and all the calculations consider three species, *i.e.*, water vapor (H_2O), oxy-

gen (O_2), and nitrogen (N_2). For the cases without mist injection, air film cooling is taken to be composed of 23% O_2 and 77% N_2 by mass. The equation for species transport is expressed as:

$$\frac{\partial}{\partial x_i}(\rho u_i C_j) = \frac{\partial}{\partial x_i}\left(\rho D_{\text{eff},j}\frac{\partial C_j}{\partial x_i}\right) + S_j \tag{12}$$

where C_j is the mass fraction of the species "j", and S_j is the source term of the species. $D_{\text{eff},j}$ is the effective diffusion coefficient.

For the discrete phase, droplets in the airflow are affected by inertia and hydrodynamic drag. Motion can be described by the second Newton's law given by the following formula:

$$m_p\frac{d\vec{v}_p}{dt} = F_d + F_g + F_o \tag{13}$$

where F_d, and F_g are the drags of the fluid on the droplet and gravity, respectively. $\bar{v}_p$ is the vectorial velocity of the droplet. F_o represents other forces, such as the thermophoretic force, the Brownian force, the Saffman's lift force and others. The vaporization rate is controlled by the concentration difference between the surface and the airstream, and the mass change rate of the droplet is calculated as follows:

$$\frac{dm_p}{dt} = \pi d^2 k_c (C_s - C_\infty) \tag{14}$$

where k_c is the mass transfer coefficient, and C_s is the vapor concentration at the saturated droplet surface. C_∞ is the vapor concentration in the bulk flow and is governed by the transport equation. Mass transfer coefficient is calculated as follows:

$$Sh_d = \frac{k_c d}{D} = 2.0 + 0.6\,Re_d^{0.5}\,Sc^{0.33} \tag{15}$$

where Sh, Re and Sc are Sherwood number, Reynolds number and Schmidt number, respectively. More details about the governing equations can be found in [13].
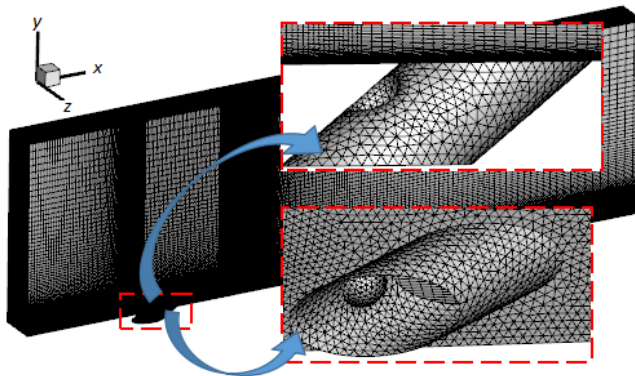

Figure 2. Meshes

Meshes and model validation

For the zone inside the film hole, unstructured grids are meshed by a multi-block method, while structured grids are used for the external channel. In addition, meshes near the blockage configuration are dense as shown in fig. 2. The first cell row for the simulated cases has a $y+$ value of 2.6.

Figure 3 shows investigations of grid dependence and model

validation by comparison of three cases with different numbers of grid cells. Compared to the results of the case with 1.2 million cells, values from the 0.32 million cells show a significant difference. Considering the similar tendency between the values for the 0.84 million cells and 1.2 million cells, the meshes with 0.84 million cells are adopted for the numerical simulations. Four thousand iterations are necessary for a specific case calculation using a computer with an E5-2680 processor of 2.7 GHz, and the calculations are convergent with residual values of 10^{-6}. Numerical simulations for the spherical blockage configurations are performed by using the software ANSYS FLUENT 16.0. Presented results were compared to the data in Huang *et al.* [19].

Figure 3. Grid independence and model validation

Results and discussion

Path lines and temperature distributions, both inside the hole and channel are illustrated in fig. 4. Path lines record trajectories of the mainstream and coolant flow. For the steady-state computations, path lines and streamlines coincide. Coolant flow bypasses the blockage configuration and is mixed with the mainstream at the hole outlet. The high temperature mainstream heats up the coolant flow fast, which results in loss of the cooling ability. For the case with the blowing ratio of 0.3, mainstream has a higher velocity than the coolant flow. A portion of the coolant flow is pushed back, and a vortex pair is formed downstream the hole position. As the diffusion between the mainstream and coolant flow disappears, downstream wall will be fully occupied by the mainstream.

Figure 4. Path lines and temperature distribution, *M* = 0.3

Figure 5 shows streamlines and temperature distributions at $x = 1d$, $x = 2.5d$, $x = 5d$ and $x = 10d$. Various cross-sections demonstrate mixing between the mainstream and coolant air in details. A kidney vortex pair is produced by the coolant jet flow. Vortices are enhanced at $x = 5d$ and weakened by the lift-off from the wall surface at $x = 10d$. When temperature distributions at the same position are compared with different blockage ratio, coolant flow is decreased with increasing blockage ratio. Moreover, a high blockage ratio causes earlier occurrence of the lift-off and greater reduction of the vortex strength.

For the blockage cases with different blowing ratios, averaged values of the lateral film cooling effectiveness are compared as shown in fig. 6. All the averaged values down
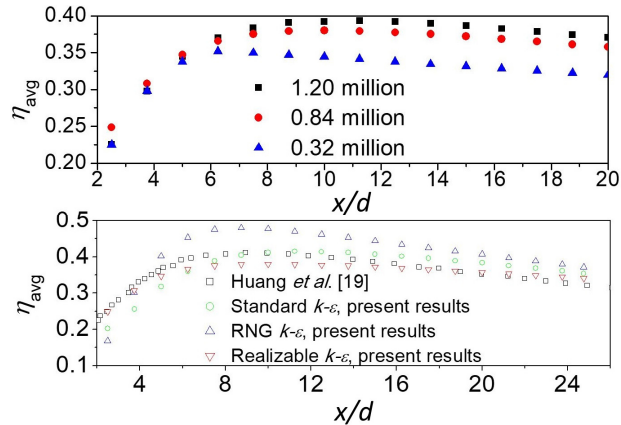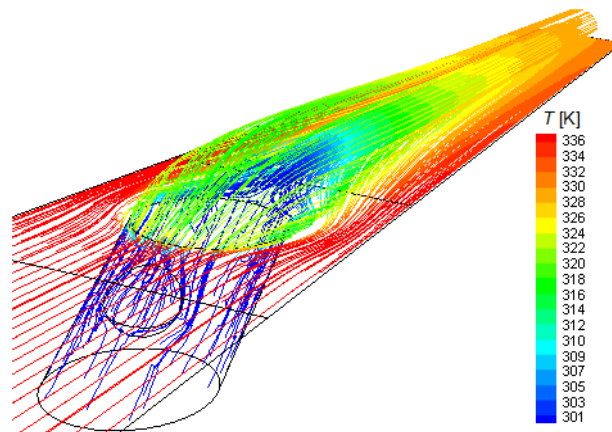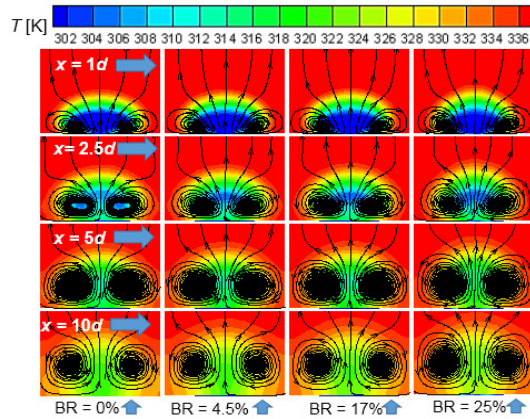
Figure 5. Streamlines and contours of temperature at different cross-sections, *M* = 0.6
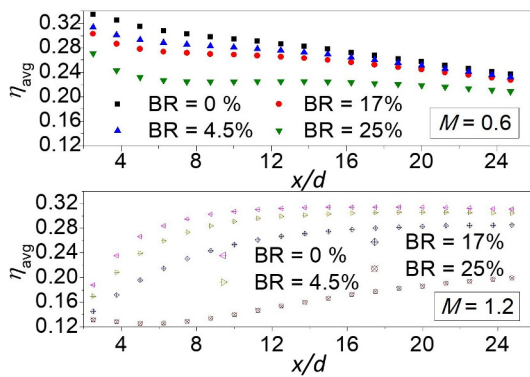

Figure 6. Comparisons of averaged lateral film cooling effectiveness for different blockage cases
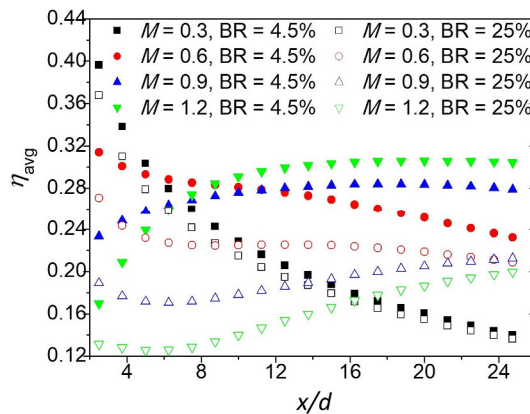

Figure 7. Lateral-averaged film cooling effectiveness for the cases with and without blockage

stream the wall monotonously decrease for the cases with a low blowing ratio and increase for the cases with a high blowing ratio. This indicates that the lateral film cooling effectiveness is strongly affected by the blowing ratio. The largest blockage ratio for the case at $M = 1.2$ shows the lowest value close to the position of $x = 5d$, while other cases present sharp improvements upstream $x = 10d$. Moreover, cooling performance deteriorates seriously when the blockage ratio reaches 25% (BR = 25%). It is also found that the lateral film cooling effectiveness decreases with increasing blockage ratio.

Cases with blockage ratios of 4.5% and 25% are used to investigate the effect of the blowing ratio, and comparison of the results at four blowing ratios is depicted in fig. 7. For the 4.5% blockage ratio (Case-S1), the averaged values of the lateral film cooling effectiveness decrease monotonically at $M = 0.3$ and $M = 0.6$, while for the blowing ratios of 0.9 and 1.2 increases sharply and then maintains almost a constant value. For the 25% blockage cases at high blowing ratios ($M = 0.9$ and $M = 1.2$), the lateral film cooling effectiveness decreases first and then increases gradually. Cases at $M = 0.3$ have a similar trend, and this implies that the 4.5% blockage ratio has a slight influence on the film cooling effectiveness. However, averaged values for large blockage cases decrease with increasing blowing ratio. This indicates that increasing the coolant flow velocity results in reduction of the lateral film cooling effectiveness for the high blockage cases.

Considering effect of mist injection, wall film cooling distributions for different blockage ratios are presented in fig. 8. For the blowing ratio of 0.6, film cooling effectiveness for the mist injection case shows higher values compared to the no mist cases. When flow velocity for the coolant air is decreased, corresponding to a lower blowing ratio, the film cooling effectiveness near

the hole location is improved significantly. However, coverage range of the cooling protection is narrower. This indicates that coolant air provides a strong entrainment capacity to carry water droplets for a long distance.

Figure 9 shows averaged values of the lateral film cooling effectiveness for the cases with and without mist injection. Based on the mass flow ratio of the coolant air at $M = 0.6$, mist injection is 1%. For the mist injection case with 4.5% blockage ratio, lateral film cooling effectiveness is improved for about 10% compared to the no mist case. When the blockage ratio is increased to 17%, mist injection provides a similar enhancement of the film cooling effectiveness. In other words, 1% mist injection results in an addition of about 10% of cooling benefit. Moreover, when a reduction of the blowing ratio occurs from 0.6 to 0.3, the lateral film cooling effectiveness for the 17% blockage case is significantly improved upstream $x = 6d$ and sharply declined downstream $x = 5d$. This indicates that low blowing ratio increases the cooling performance in the vicinity of the hole location, whereas the maintenance of cooling ability is significantly weakened.

Figure 8. Film cooling effectiveness for the 17% blockage case with and without mist injection
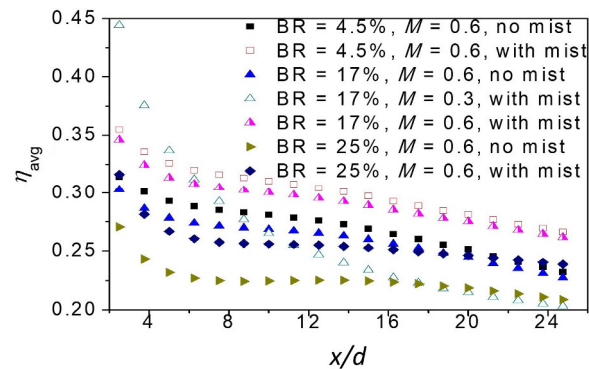
Figure 9. Lateral-averaged film cooling effectiveness for cases with and without mist injection

Conclusions

Film cooling characteristics were numerically investigated in a rectangular channel by using the realizable k-ε turbulence model. Moreover, discrete phase model was used to analyze the effect of the mist injection on the cooling benefits. The flow distribution and film cooling effectiveness for various blockage and blowing ratios were examined in details. Major findings can be summarized as follows:
(1) the lift-off and the reduction of the vortex strength occur earlier for a high blockage ratio than for a low BR; for the large blockage cases (BR = 25%), the lateral film cooling effectiveness decreases with increasing blowing ratio,
(2) the lateral coverage area of the coolant flow is decreased with an increase in the BR; for the case at $M = 1.2$, the 25% blockage case shows the lowest lateral cooling performance near $x = 5d$, and
(3) for the spherical blockage cases, an extra cooling benefit of 10% is obtained by injecting 1% water droplets into the coolant flow; lateral film cooling effectiveness for $M = 0.3$ is improved near the film hole but weakened downstream the wall.

The objective of this study is to propel the profound understanding of the usefulness of injecting water droplets into the coolant flow. A theoretical analysis of the effect between
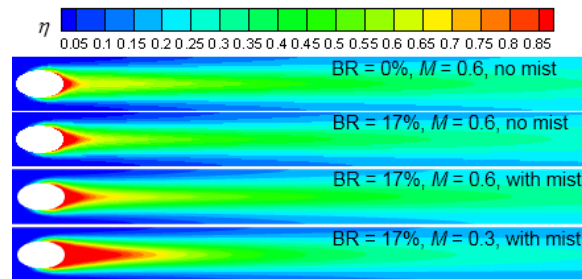
the blockage and the mist injection is provided. The film cooling with the mist injection is first investigated based on the partial blockage hole. It is suggested that the gas turbines should lower the blockage ratio, and the injection of the water droplets is also recommended when the blockage cannot be avoided. The findings can be used in other engineering applications where the cooling protection is needed to be investigated.

Acknowledgment

Nomenclature

BR	– blockage ratio, [–]	ε	– turbulence dissipation rate, [m^{-2}s^{-3}]
c_p	– specific heat, [Jkg^{-1}K^{-1}]	η	– adiabatic film cooling effectiveness,
d	– diameter of film hole, [m]		$[= (T_{aw} - T_m)/(T_c - T_m)]$, [–]
F	– force, [N]	λ	– thermal conductivity, [Wm^{-1}K^{-1}]
k	– turbulence kinetic energy, [m^{2}s^{-2}]	μ	– dynamic viscosity, [kgm^{-1}s^{-1}]
k_c	– mass transfer coefficient, [ms^{-1}]	ρ	– density, [kgm^{-3}]
M	– blowing ratio, [$= \rho_c V_c/\rho_m V_m$]	τ	– stress tensor, [kgm^{-1}s^{-2}]
m	– mass, [kg]		
P	– pressure, [Nm^{-2}]	*Subscripts*	
S	– source term, [–]		
T	– temperature, [K]	aw	– adiabatic wall
u	– stream-wise velocity component,	b	– blockage
	[ms^{-1}]	c	– coolant jet
		m	– mainstream flow
V	– velocity magnitude, [ms^{-1}]	p	– droplet
x, y, z	– coordinates, [m]	s	– droplet surface
		t	– turbulent

Greek symbols

α – inclination angle, [deg]

References

[1] Kumar, M., *et al.*, Conjugated Heat Transfer Analysis of Gas Turbine Vanes Using MacCormack's Technique, *Thermal Science*, *12* (2008), 3, pp. 65-73
[2] Liu, X., Zheng, H., Influence of Deflection Hole Angle on Effusion Cooling in a Real Combustion Chamber Condition, *Thermal Science*, *19* (2015), 2, pp. 645-656
[3] Xie, Y. H., *et al.*, Numerical Study on Film Cooling and Convective Heat Transfer Characteristics in the Cutback Region of Turbine Blade Trailing Edge, *Thermal Science*, *20* (2016), Suppl. 3, pp. 643-649
[4] Koc, I., *et al.*, Numerical Investigation of Film Cooling Effectiveness on the Curved Surface, *Energy Conversion and Management*, *47* (2006), 9, pp. 1231-1246
[5] Asghar, F. H., Hyder, M. J., Computational Study of Film Cooling From Single and Two Staggered Rows of Novel Semi-Circular Cooling Holes Including Coolant Plenum, *Energy Conversion and Management*, *52* (2011), 1, pp. 329-334
[6] Bayraktar, S., Yılmaz, T., Three-dimensional Analysis of Temperature Field for Various Parameters Affect the Film Cooling Effectiveness, *Energy Conversion and Management*, *52* (2011), 4, pp. 1914-1929
[7] Shine, S. R., *et al.*, Internal Wall-jet Film Cooling with Compound Angle Cylindrical Holes, *Energy Conversion and Management*, *68* (2013), 3, pp. 54-62
[8] Du, K., Li, J., Numerical Study on the Effects of Slot Injection Configuration and Endwall Alignment Mode on the Film Cooling Performance of Vane Endwall, *International Journal of Heat and Mass Transfer*, *98* (2016), July, pp. 768-777
[9] Sheng, L., Hao, Y. L., Particle Deposition Characteristics in Entrained Flow Coal Gasifier, *Thermal Science*, *16* (2012), 5, pp. 1544-1548

Wang, J., *et al.*: Effect of Spherical Blockage Configurations on Film Cooling…

10   THERMAL SCIENCE: Year 2018, Vol. 22, No. 5, pp. XXXX-XXXX

[10] Chung, H. Y., *et al.*, Trailing Edge Cooling of a Gas Turbine Blade with Perforated Blockages with Inclined Holes, *International Journal of Heat and Mass Transfer*, *73* (2014), 3, pp. 9-20

[11] Davidson, F. T., *et al.*, A Study of Deposition on a Turbine Vane with a Thermal Barrier Coating and Various Film Cooling Geometries, *ASME Journal of Turbomachinery*, *136* (2013), 4, pp. 1769-1780

[12] Kistenmacher, D. A., *et al.*, Realistic Trench Film Cooling with a Thermal Barrier Coating and Deposition, *ASME Journal of Turbomachinery*, *136* (2014), 9, pp. 091002

[13] Li, X. C., Wang, T., Simulation of Film Cooling Enhancement with Mist Injection, *ASME Journal of Heat Transfer*, *128* (2006), 6, pp. 509-519

[14] Wang, J., *et al.*, Effects of Deposition Locations on Film Cooling with and without a Mist Injection, *Numerical Heat Transfer Part A- Applications*, *70* (2016), 10, pp. 1072-1086

[15] Wang, J., *et al.*, Effects of Surface Deposition and Droplet Injection on Film Cooling, *Energy Conversion and Management*, *125* (2016), Oct., pp. 51-58

[16] Wang, J., *et al.*, Effects of Deposition Height and Width on Film Cooling, *Numerical Heat Transfer Part A- Applications*, *70* (2016), 6, pp. 673-687

[17] Pan, C. X., *et al.*, Numerical Investigation of Partial Blockage Effect on Film Cooling Effectiveness, *Mathematical Problems in Engineering*, *2014* (2014), Article ID 167193, p. 13

[18] Yang, C. F., Zhang, J. Z., Experimental Investigation on Film Cooling Characteristics from a Row of Holes with Ridge-shaped Tabs, *Experimental Thermal and Fluid Science*, *37* (2012), 3, pp. 113-120

[19] Huang, K. N., *et al.*, Effect of Partial Blockage Inside Film Hole on Film Cooling Characteristics, *Journal of Aerospace Power*, *29* (2014), 6, pp. 1330-1338

[20] Wilcox, D. C., *Turbulence Modeling for CFD*, DCW Industries Inc., La Canada, California, United States of America, 2006

[21] Versteeg, H. K., Malalasekera, W., *An Introduction to Computational Fluid Dynamics – The Finite Volume Method*, Longman, London, United Kingdom, 2007